Received: 13 June 2023 | Revised: 14 August 2023 | Accepted: 24 August 2023

DOI: 10.1002/hyp.14988

RESEARCH ARTICLE

WILEY

Improved understanding of vegetation dynamics and wetland ecohydrology via monthly UAV-based classification

Songjun Wu [1,2] | Doerthe Tetzlaff [1,2,3] | Hauke Daempfling [1] | Chris Soulsby [1,3]

[1]Department of Ecohydrology, Leibniz Institute of Freshwater Ecology and Inland Fisheries, Berlin, Germany

[2]Department of Geography, Humboldt University Berlin, Berlin, Germany

[3]Northern Rivers Institute, School of Geosciences, University of Aberdeen, Aberdeen, UK

Correspondence
Songjun Wu, Department of Ecohydrology, Leibniz Institute of Freshwater Ecology and Inland Fisheries, Berlin, Germany.
Email: songjun.wu@igb-berlin.de

Funding information
Chinese Scholarship Council (CSC); Einstein Foundation Berlin and Berlin University Alliance, Grant/Award Number: ERU-2020-609; Leverhulme Trust, Grant/Award Number: RPG 2018 375

Abstract

Vegetation classification is an essential prerequisite for understanding vegetation-water relations at a range of spatial scales. However, in site-specific applications, such classifications were mostly based on a single Unmanned Aerial Vehicle (UAV) flight, which can be challenging in grasslands and/or herbaceous-dominated systems, as those communities are small in size and highly mixed. Here, we conducted monthly UAV flights for two years in a riparian wetland in Germany, with acquired imagery used for vegetation classification on a monthly basis under different strategies (with or without auxiliary information from other flights) to increase understanding in eco-hydrology. The results show that multi-flight-based classification outperformed single-flight-based classification due to the higher classification accuracy. Moreover, improved sensitivity of temporal changes in community distribution highlights the benefits of multi-flight-based classification - providing a more comprehensive picture of community evolution. From reference to the monthly community distribution, we argue that a combination of two or three flights in early- and late-summer is enough to achieve comparable results to monthly flights, while mid-summer would be a better timing in case only one flight is scheduled. With such detailed vegetation mapping, we further interpreted the complex spatio-temporal heterogeneity in NDVI and explored the dominant areas and developmental progress of each community. Impacts from management (mowing events) were also evaluated based on the different responses between communities in two years. Finally, we explored how such vegetation mapping could help understand landscape ecohydrology, and found that the spatio-temporal distribution of minimal soil moisture was related to NDVI peaks of local community, while grass distribution was explained by both topography and low moisture conditions. Such bi-directional relationships proved that apart from contributing to an evidence base for wetland management, multi-flight UAV vegetation mapping could also provide fundamental insights into the ecohydrology of wetlands.

KEYWORDS

ecohydrology, remote sensed vegetation dynamics, soil moisture, UAV, unmanned aerial vehicles, wetlands

1 | INTRODUCTION

Vegetation-water interactions are of central interest to the field of ecohydrology as vegetation exerts a key control on hydrological partitioning and the water cycle (Tabacchi et al., 2000). Vegetation communities obviously need water to survive, grow and reproduce, and thus, their distribution, structure and phenology are directly influenced by spatio-temporal patterns of water availability (Dumont et al., 2012). Moreover, vegetation is usually the primary conduit for returning terrestrial water to the atmosphere via transpiration, while also affecting albedo and canopy roughness (Chapin et al., 2011), which in turn exert a strong effect on the local energy balance and hydrological fluxes. Especially given the increased development and application of distributed ecohydrological models in recent years (Wellen et al., 2015), detailed mapping of vegetation cover, regarding both spatial distributions and phenological dynamics, have powerful potential for informing and improving such models; particularly in terms of providing valuable constraints on vegetation-water interactions, and contributing to an evidence base for better quantifying the hydrological impacts of current and future land management at a range of spatial and temporal scales (Rapinel et al., 2019).

Remote sensing offers a practical, rapid and economic means of vegetation mapping (Nordberg & Evertson, 2005). As a direct product of remote sensing, numerous vegetation indices (VIs) have been widely explored for characterizing vegetation (e.g., productivity etc.) (Pettorelli et al., 2005). For instance, the relationship between the normalized difference vegetation index (NDVI) and the fraction of absorbed photosynthetic active radiation (fAPAR) has been well documented both theoretically (Sellers et al., 1992) and empirically (Asrar et al., 1984). Therefore, NDVI has been widely used as a proxy to assess vegetation productivity and phenological patterns in many terrestrial ecosystems (Kariyeva & van Leeuwen, 2011; Nemani et al., 2003; Wu et al., 2017; Yu et al., 2003). Furthermore, benefiting from the development of Unmanned Arial Vehicle (UAV)-borne sensors in recent years, NDVI can be mapped at ultra-high resolution for smaller scale assessment, which has proved to be informative and supportive for precision farming and other agricultural applications (Candiago et al., 2015; Yeom et al., 2019).

However, in less intensively managed systems, which are different from arable land where more homogenous crops are dominant, the spatial patterns are generally more complicated and exhibit higher temporal variability (Cole & Sheldon, 2017; Donaldson & Lindroth, 2008; Roth et al., 2015). For example, in complex riparian wetlands dominated by various grass and herbaceous communities/species - which are small in size and highly mixed (Bradter et al., 2019) - extracting information from NDVI maps is often problematic due to the extreme spatial heterogeneity.

In this context, vegetation classification can be advantageous, as it can downscale the VI analysis to the community or species level, whose distribution is the major cause of such spatial heterogeneity. Many classification applications have been conducted based on UAV-acquired imagery in grass-dominated ecosystems (Table 1), which generally followed a similar workflow: (i) image pre-processing, (ii) image segmentation (for object-based analysis), (iii) feature extractions, and (iv) classification/validation (Belgiu & Drăgu, 2016; Xie et al., 2008). Some of the applications achieved strong performance, for example, high accuracies were achieved with only spectral information (but without including auxiliary data such as topography, soil type) in Bradter et al. (2019). However, many studies still acknowledged the challenges in vegetation classifications, which mainly originate from the spectral and structural similarities of different grass or herbaceous species, resulting in low classification accuracies (Geerling et al., 2007). Moreover, the spectral separability is not only affected by vegetation, but also the site conditions (Pottier et al., 2014); as the spectra is inherently associated with the soil cover and water content (Feilhauer & Schmidtlein, 2011), while heterogeneity of these environmental variables can also affect the vegetation phenology due to their close coupling with local soil properties and moisture availability (Dumont et al., 2012; Marion et al., 2010). In addition, when anthropogenic activities such as grazing or grassland management (e.g., mowing, fertilization etc.) are involved (Dumont et al., 2012), vegetation-spectral associations are usually further complicated, and thus, impede precise mapping (Dirnböck et al., 2003).

Therefore, to date, remotely-sensed vegetation classification is still often problematic even with high-resolution UAV-acquired imagery. Although a wide range of previous studies have explored alternative aspects of UAV-based classification, such as data sources [*visual spectral* (Pande-Chhetri et al., 2017), *multispectral* (Komarek et al., 2018); *hyperspectral* (Yan et al., 2019) *and texture indices* (Laliberte & Rango, 2009)], image analysis method [*objective-* (Ahmed et al., 2017) *or pixel-based* (Hamylton et al., 2020)], classification algorithms [*statistics* (López-Granados et al., 2016) *or machine/deep learning algorithms* (Palace et al., 2018)] and classification targets [*species discrimination* (Komarek et al., 2018) *or identification of invasive species* (Baron & Hill, 2020)], a general and transferable method is still lacking due to the complex relationship between spectra and vegetation species/communities.

A potential solution to clarify the complex relationships is to use multi-temporal imagery instead of single-date imagery, as the different degrees of variation in spectra through the seasons help differentiate the vegetation species/communities (Andrew & Ustin, 2008; Laba et al., 2005). However, such applications are usually conducted with satellite imagery owing to the relatively low costs for image acquisition at a high frequency (Bradter et al., 2019; Senf et al., 2015; Son et al., 2013; Wang et al., 2013; Weisberg et al., 2021), while UAV-based studies are emerging but still very limited (e.g., Müllerová et al., 2017; van Iersel et al., 2018; Weil et al., 2017). For example, the application in van Iersel et al. (2018) benefited from the auxiliary data from multi-temporal flights, that is, including multispectral-based vegetation indices and vegetation heights from six different flights, which increased the classification accuracy to 99.3%. Similarly, Weil et al. (2017) successfully classified woody vegetation species using UAV-acquired imagery at five different dates and weekly NDVI time series from a near-surface camera; while Weisberg et al. (2021) used spectral information from 8 flights in growing seasons to identify two invasive species. These studies demonstrated the advantages of multi-temporal flight missions; however, most of the applications have either relatively low temporal frequency (i.e., limited coverage of

TABLE 1 Overview of recent studies of vegetation classification in grass-dominated ecosystem based on UAV imagery.

Input datasets	Classes/objective	Res. (cm)	Classifer	References
R, G, B	Several grass, shrub, forest species	8	SVM/ANN	(Pande-Chhetri et al., 2017)
R, G, B	2 grass and 3 shrub species	6	KNN	(Laliberte, Winters, & Rango, 2011)
R, G, B	Grass, shrubs, forest	10	SVM/RF	(Wang et al., 2019)
R, G, B	9 wetland vegetation categories	5	ANN	(Zweig et al., 2015)
R, G, B	Grass, shrub, and forest	<8	T	(Zhang et al., 2019)
R, G, B, RE, NIR	Several grass and shrub species	14	KNN	(Laliberte, Goforth, et al., 2011)
R, G, B, texture indices	Shrub and grass	5	DT	(Laliberte & Rango, 2009)
R, G, B, texture indices	5 grass and shrub categories	~1	ANN	(Palace et al., 2018)
R, G, B, NIR, texture indices	Several forest, shrub, herbaceous species	4–13	RF	(Ahmed et al., 2017)
G, R, RE, NIR, multi-band indices, texture indices	Fraction of *centaurea maculosa*	2.9	RF	(Baron & Hill, 2020)
R, G, B, RE, NIR, texture indices	Sunflower and weeds	2–5	Others[a]	(López-Granados et al., 2016)
R, G, B, RE, NIR, LWIR	2 grass and 15 forest species	3–18	SVM	(Komarek et al., 2018)
Hyperspectral data and camera angles	3 herbaceous and 2 forest species	4	DT	(Yan et al., 2019)
Hyperspectral data	Young/intermediate/old grassland	100–500	PLSR	(Astor et al., 2014)
R, G, B, NIR, texture indices in 2 time steps	2 invasion grass species	50	SVM/RF	(Müllerová et al., 2017)
R, G, B, NIR, DSM in 6 time steps	6 herbaceous and grassland species	5	RF	(van Iersel et al., 2018)
R, G, B in 4 time steps (10 years interval)	Detection of *Lomandra*	3	CNN	(Hamylton et al., 2020)
R, G, B, NIR, texture indices in 4 time steps	4 grass species	~5	RF	(Lu & He, 2017)
R, G, B, NIR, RE, LWIR, DSM, texture (monthly)	4 grass species and forest	10	RF	This study

Abbreviations: KNN, k-nearest neighbours algorithm; PLSR, partial least squares regression; SVM, support vector machine; T, threshold-based classification.
[a]Others: stepwise threshold classification.

seasonal differences) or limited temporal/spatial coverage. To authors' knowledge, mapping at monthly frequency spanning two years is still rare. Accordingly, guidance on UAV flight strategies on *how to use fewer flights to obtain still representative results over longer periods like an entire year (acquired from monthly flights)*, is generally missing.

Therefore, in this study, multi-temporal UAV flights and simultaneous field surveys were conducted on a monthly basis over two years (01.2021–12.2022) in a fen peatland/wetland in Germany. With multi-spectral imagery and field surveys covering different seasons, the vegetation was classified each month at the community level. Then we investigated the spatio-temporal pattern of vegetation productivity by summarizing the NDVI for each community, and evaluated the impacts of management owing to the occurrence of two major mowing events. The links between classified results (community distribution and phenological dynamics) and soil moisture were further investigated. The overarching goal of this study was to assess the value of multi-temporal UAV flights, to downscale the monthly vegetation dynamics into community level, and to investigate their relationships to the site hydrology. The specific research questions were:

- Can data fusion from multi-temporal flight assist UAV-based vegetation classification in a complex wetland?
- What are the spatial patterns and temporal dynamics in vegetation productivity and their response to the land use management? How can vegetation classification improve such evaluation?
- What are the implications of multi-temporal, detailed vegetation mapping for understanding landscape ecohydrological processes?

2 | MATERIALS AND METHODS

2.1 | Study area

The studied wetland is located in a long-term experimental catchment (the Demnitzer Millcreek catchment, DMC; Figure 1b) in north-eastern Germany (52°25′ N, 14°14′ E). The riparian area is a peat fen dominated by histosols (1–4 m deep) and traversed by a ~ 2.1 km stream, while areas at the edge of the fen are characterized by sandy brown earth soils. The peat has been drained historically by a network of ditches feeding the central river channel. The vegetation distributions are also closely related to the proximity to the stream network, with grass and herbaceous communities dominating the riparian peaty area (though highly diverse and mixed) while forests are distributed on the sandy soils (Wu et al., 2021).

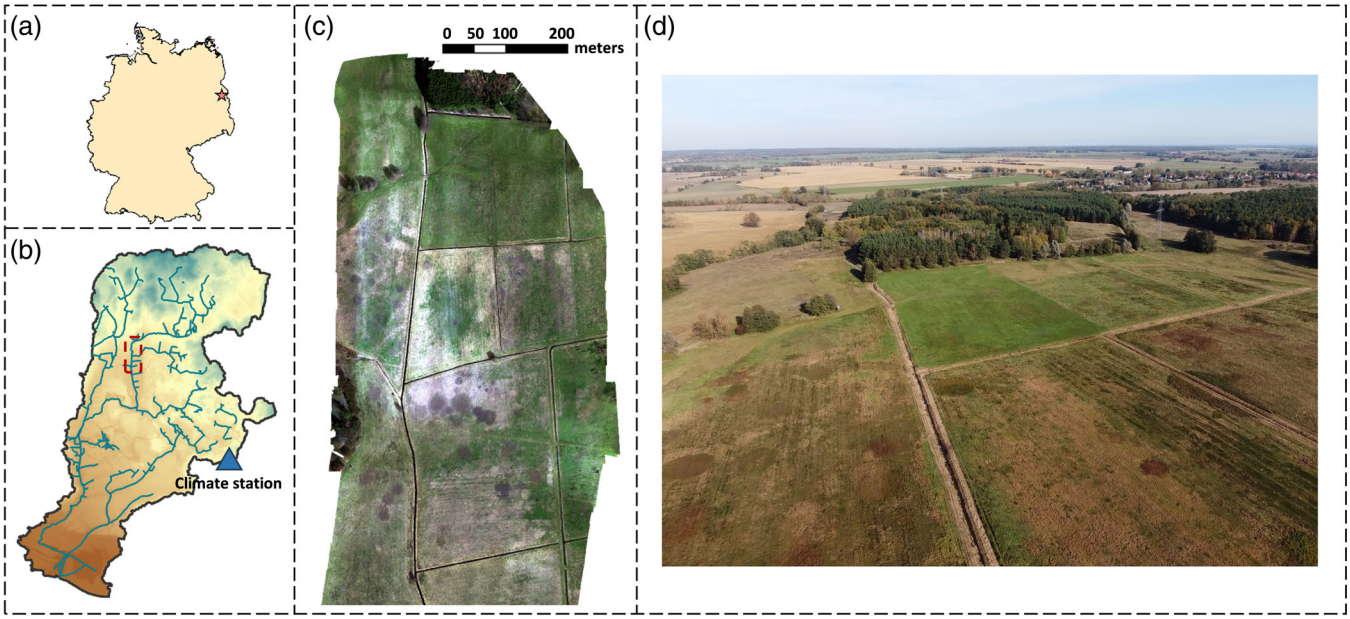

FIGURE 1 The study area located in (a) NE Germany, (b) the Demnitzer Millcreek catchment. Subplot (c) shows the true colour image from a flight in early spring (30.03.2021) of the study area, while subplot (d) shows the overview captured by a visual camera.

The area experiences a humid continental climate with a modest annual precipitation (~570 mm/year), energy input (average net radiation of ~52.9 W/m^2), and higher potential evapotranspiration (650–700 mm/year) than rainfall (Smith et al., 2021). These hydroclimatic conditions formalized relatively dry conditions across the wetland in summer, which have been further exacerbated by a prolonged period of below-average rainfall since 2013, and reflected by relatively low annual discharge (0.02 and 0.06 m^3/s at inlet and outlet of the study area) (Wu, Tetzlaff, Goldhammer, et al., 2022).

The anthropogenic impacts of grassland management stem mainly from mowing events, which generally took place in summer (between July and August). However, the timing and the mowing areas are not constant over the years, as they mainly depend on how much grass and area are needed for sheep grazing (which are decided by local farmers and stakeholders).

2.2 | UAV imagery acquisition, pre-processing and vegetation indices

UAV flights were conducted to collect multi-spectral imagery in NADIR conditions over the wetland on a monthly basis from 03.2021 to 12.2022 with occasional gaps (20 flights in total). The UAV platform used was the Matrice 210 V2 RTK, DJI. For each flight, the studied wetland and surrounding forests were covered by four sequential sub-flights from north to south. The areas of these sub-flights were delineated by waypoints in the flight control system (DJI Pilot flight planning), from which flight paths were generated to ensure that the adjacent flights have ~10% of overlapping area. All settings were fixed after the first flight in order to retain the identical area and pathways for the following missions.

The imaging sensor used in this study was a Micasense Altum camera. It has a resolution of 3.2 megapixels, and provides imagery in six multi-spectral center wavelengths and bandwidths: blue (475 nm, 32 nm), green (560 nm, 27 nm), red (668 nm, 16 nm), red edge (717 nm, 12 nm), near infrared (840 nm, 57 nm) and longwave infrared (11 μm, 6 μm; the thermal sensor has lower resolution 160 × 120 than the other channels). During each mission, the UAV was flown with relatively stable mid-day illumination (11 a.m. to 2 p.m.) at an altitude of 100 m above ground, the maximum height allowed by the airspace authority at the time. This resulted in a high spatial resolution of images (~5 cm). The forward and side overlapping of images were 80% and 75%, respectively.

The flight paths were controlled by the UAV's onboard RTK system and ground reference station (DJI D-RTK 2). All images were georeferenced by the on-board GPS receiver of the camera. Moreover, the radiometric reference of the six bands were taken before and after each sub-flight (eight references in total) and the camera's companion downwelling light sensor (Micasense DLS2) measured sun-to-sensor angle and direct and diffuse irradiance components.

The image processing was conducted using Pix4Dmapper on a high-performance desktop (Intel(R) Xeon(R) W-1290P CPU @ 3.70GHz with 128GB RAM and an NVIDIA GeForce RTX 3090 graphics card) to obtain the reflectance maps of six bands. Images from each of the four flights were processed individually for reflectance maps of the six bands and a digital surface model (DSM) using structure-from-motion (SfM) photogrammetry (Schonberger & Frahm, 2016). To merge the processed maps more accurately, around 20 ground control points collected over the wetland in winter time (October and December 2021) were used, while in other seasons, manual tie points were sampled via on-screen digitizing in Pix4Dmapper due to the difficulty of placing ground control points over the

dense vegetation. The missing of ground control points resulted in uncertainty in absolute values of DSM, but the relative DSM was convincing due to the use of RTK and manual tie points. The radiometric calibration was conducted iteratively against eight references collected during the flights to exclude the references producing abnormal results. Accordingly, calibration against the remaining references all led to similar results, and one reference was selected to generate the reflectance maps. Based on the reflectance, monthly maps of normalized difference vegetation index (NDVI) were calculated as a proxy of vegetation productivity:

$$NDVI = \frac{Nir - Red}{Nir + Red}$$

2.3 | Vegetation classification and interpretation

2.3.1 | Reference data collection

A medium thematic resolution containing five different vegetation communities (i.e., grassland, early-season low herbaceous, late-season low herbaceous, high herbaceous, and forest) was selected based on their structure and phenological characteristics. For the definition and species composition for each community please refer to Table 2.

During each flight mission in 2021, the dominant community was identified at ~50 sites that were evenly distributed across the study area, with coordinates recorded using handheld GPS (Garmin eTrex 30X). Photos of the surrounding environment were also taken for a wider estimate of community distributions. Then, ~500 samples were complemented based on the photos via on-screen digitizing, which is common in UAV-based classifications (Lu & He, 2017; van Iersel et al., 2018). Some classes (i.e., forest, shadow, and water surface) only had few ground true points (<5) from the field surveys and were mainly sampled by on-screen digitizing; however, they were generally distinct either in the DSM or spectral information and easily identifiable on the maps.

TABLE 2 The description and species composition of each community.

Community	Description	Species composition
Grassland	Sparse grass community with height <30 cm	Fescue (*Festuca*), ryegrass (*Lolium*)
Early-season low herbaceous	Herbaceous community with height between 30 and 60 cm; mainly exists in early summer	Chee Grass (*Stipa splendens*), ryegrass (*Lolium*)
Late-season low herbaceous	Herbaceous community with height between 30 and 60 cm; mainly exists in late summer	Nut Grass (*Cyperus rotundus*), ryegrass (*Lolium*)
High herbaceous	Herbaceous community with height >60 cm	Nettle (*Urtica dioica*), ryegrass (*Lolium*), reed (*Phragmites australis*)
Forest	Forest community	Scots Pine (*Pinus*), etc.

In addition to vegetation-related data, hydrological characteristics were also investigated during each flight by measuring moisture content in the upper soil layer (top 10 cm) via a handheld soil moisture probe (ML3 ThetaProbe Sensor, Delta-t, Germany) at ~30 sites that were randomly selected but evenly distributed across the study area, with coordinates recorded using handheld GPS.

2.3.2 | Classification workflow

The vegetation classification was realized using object-based image analysis, which is more robust than pixel-based analysis for fine-resolution classification (Modica et al., 2021). This includes three major steps, that is, image segmentation, feature extraction and random forest classification (Figure 2). The entire workflow was built in Python (available at: https://github.com/songjun-wu/Vegetation-classification.git) and is briefly described here.

First, the imagery was segmented into objects using an open-source algorithm (Shepherd algorithm; Shepherd et al., 2019) implemented in the Remote Sensing and Geographical Information Systems software library (RSGISLib; Bunting et al., 2014). The algorithm has been tested in Modica et al. (2021), which achieved an equivalent performance for high-resolution segmentation compared to commonly used Large-Scale Mean-Shift algorithm in Orfeo ToolBox and Multi-Resolution Segmentation in eCognition. Briefly, the segmentation is realized based on an iterative elimination method consisting of three steps: (a) applying K-means clustering (McQueen, 1967) to identify the unique spectral signatures within the image and assign pixels to the associated cluster center; (b) then a clumping process was conducted to create unique regions; finally, (3) objects were formalized by iteratively removing regions below the minimum pixels and merging them to the neighbouring clumps that are spectrally closest (assessed through the Euclidean distance) (Shepherd et al., 2019). The key parameters were set via trial-and-error, whose description and selected values were shown in Table 3. Note that the optimized values may vary between imageries with different complexities or resolutions.

Then, features were extracted for segmented objects. Due to the availability of UAV-acquired data at multiple dates, three different strategies were selected for classification (Figure 2).

Strategy 1 (S1): like most applications which are based on a single-date data source (Kumar & Sinha, 2014; Martínez-López et al., 2014), this classification was conducted on the datasets on that date. The main features used for classification include the mean and standard deviation of six spectral bands, DSM, and four more vegetation indices (NDVI, Blue-NDVI, Green-NDVI, and Rededge-NDVI, see description in Table 4). The texture indices, which are the second-order statistics derived from the grey-level co-occurrence matrix (GLCM), were also incorporated into model training as well, which was shown previously to assist classification in several high-resolution applications (Baron & Hill, 2020; Laliberte & Rango, 2011). For full description of selected features please refer to Table 4.

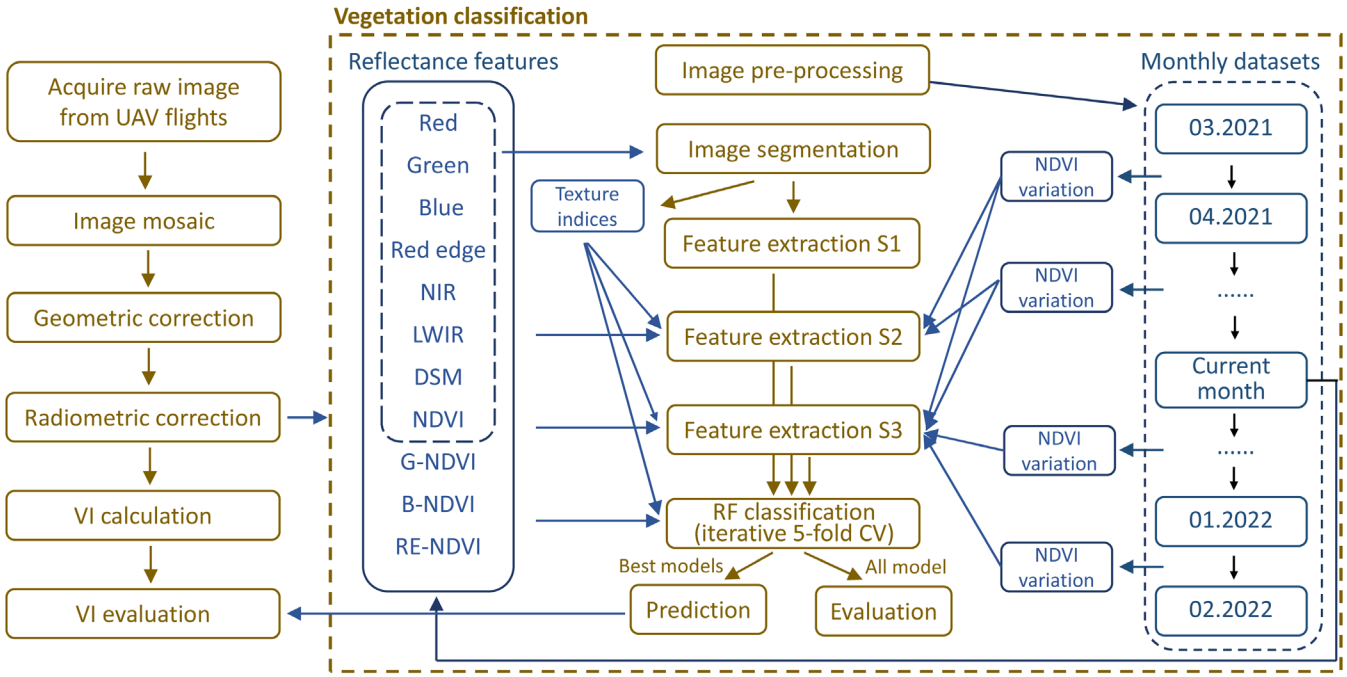

FIGURE 2 Main workflow of the vegetation classification. The input datasets and key procedures are shown in blue and brown, respectively.

TABLE 3 The key parameters in object-based image segmentation.

Parameter	Value	Description
numClusters	20	The number of clusters within the K-Means clustering
samplingNum	70	The subsampling of image data used within the K-Means
minPxls	200	The minimum number pixels within an object
kmMaxIter	3000	Maximum iterations for K-Means

Strategy 2 (S2): Apart from the basic features extracted in S1, a data fusion from previous flights was conducted for model training. Unlike previous studies which directly used the spectral information from other dates (e.g., Rapinel et al., 2019 or Weisberg et al., 2021), we calculated monthly NDVI variations instead. The variations of previous and current months were included in classification in this strategy.

Strategy 3 (S3): The classification was conducted using features in S1 plus the aforementioned NDVI variations, regardless of whether they (i.e., the variations) originated from the dates before or after current flight.

Finally, the extracted features (Table 4) were used for vegetation classification using a Random Forest Classifier (Pal, 2005), with hyperparameters determined via trial-and-error approach: the number of trees in models was set as 5000 due to the availability of computational capacity (parallel use of >50 cores in the high performance computer cluster from Humboldt University Berlin), while the maximum depth of the tree was set to 20 to avoid overfitting. For images acquired at different times, classification models were established separately, since there were considerable temporal changes of classes. This resulted in monthly maps of vegetation distribution.

Further, to prevent impacts from sample selection, 5-fold cross-validations were repeated for 10 occasions (Rapinel et al., 2019). The average accuracy of either each individual class or all classes was calculated, and the best performing model was selected based on overall accuracy for further prediction.

2.3.3 | Summary of community phenology

Since nine vegetation maps were produced in 2021 (Figure 6), the spatial dominance of each community could be summarized based on its temporal frequency of occurrence on a monthly basis. More specifically, for each pixel, the dominant community was defined as the most frequent community if it was detected more than four times over the nine sets of classification results. Otherwise, the pixel was characterized as grassland. Then, the NDVI was extracted and summarized from the dominant area of each community. The classified vegetation distribution was also used to extract NDVI in 2022, which could result in uncertainty if vegetation communities switch dramatically between years. However, based on our field-based observations and knowledge from weekly sampling since 2019, the vegetation evolution is relatively stable interannually at our site. Additional on-screen verification of the vegetation distribution in 2022 was also conducted to ensure the creditability of our results.

TABLE 4 Features selected for image segmentation.

Abbreviation	Description
B[b]	Band blue
G[b]	Band green
R[b]	Band red
RE[b]	Band red edge
NIR[b]	Band near infrared
T[b]	Surface temperature calculated from long-wave radiation
DSM[b]	Digital surface model estimated via structure-from-motion photogrammetry
NDVI[b]	Normalized difference vegetation index: (NIR-R)/(NIR + R)
B-NDVI[b]	Normalized difference blue index: (NIR-B)/(NIR + RE)
RE-NDVI[b]	Normalized difference red edge index: (NIR-RE)/(NIR + RE)
contrast_GLCM	The intensity contrast between pixels within an object
dissimilarity_GLCM	A measure of distance between pairs of pixels
homogeneity_GLCM	The closeness of the element distribution of in an object to its diagonal
energy_GLCM	The sum of squared elements
correlation_GLCM	Grey-tone linear-dependencies in the image
ASM_GLCM	Angular second moment: a measure of homogeneity of the image
Δ NDVI month[a]	The NDVI change of an object from last month: $NDVI_{(month)} - NDVI_{(month-1)}$
Max NDVI date	The date of occurrence of maximum NDVI value within an object
Average NDVI[a]	The average NDVI over whole sampling period (differs between S2 and S3)

[a]The feature was extracted as the average value within the segmented object.
[b]Means both mean and standard deviation were extracted.

3 | RESULTS

3.1 | Meteorological background of flight missions

Precipitation, air temperature, wind speed, and air pressure were measured every 15 min at a climate station ~ km away from the wetland (Station Alt Madlitz, Figure 1). Potential evapotranspiration (PET) was estimated via the Penman–Monteith equation (Penman, 1948) using these variables. The climatic indices showed clear seasonal patterns (Figure 3): air temperature and PET gradually increased after March in both years and reached maxima (28.0°C and 7.6 mm/d) in July. The subsequent decline started in late August. As for precipitation, the winter season was characterized by frequent but less intense frontal events, while summer rainfall was mainly in the form of sporadic convective events with higher intensity.

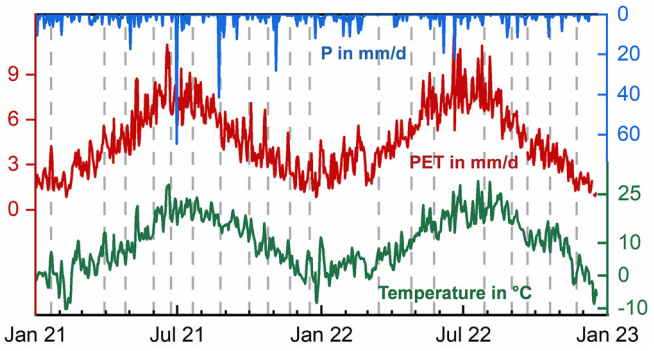

FIGURE 3 Daily precipitation (P in blue), potential evapotranspiration (PET in red), and air temperature (T in green). The dates of flight missions are shown as grey lines.

The inter-annual differences showed drier and warmer conditions in 2022 compared to 2021. This was reflected by 44.0% decrease in annual precipitation and 9.7% increase in temperature in 2022, which was partly due to the two intense summer events in 2021 when the precipitation amount reached >80 mm in June and August.

3.2 | Assessing vegetation classification based on different strategies

3.2.1 | Classification accuracy

The overall accuracies of classification gradually increased after incorporating the temporal dynamics of NDVI (from S1 to S3), but all three strategies achieved relatively high accuracies with average values of 87.0%, 92.9%, and 94.7% for S1, S2, and S3, respectively (Figure 4). The accuracy slightly decreased in growing seasons, but still remained above 80% (84.2%, 89.5%, and 91.1%).

In terms of individual classes, forest could be most effectively differentiated from other classes with accuracies close to 100% (98.0%, 98.9%, and 99.0% for S1, S2, and S3), while grassland and early-season herbaceous classes were more difficult to identify. For instance, the accuracies of classifications based on S1 for early-season low herbaceous were below 80% in May and August, mainly because of the similar spectral reflectance to grassland. Accordingly, the classification of grassland was less accurate in both months (78.0% and 83.8%).

However, the data fusion from other flights assisted the differentiation between these two classes, leading to increased accuracies in these two months (93.0/90.1% and 96.5/95.0% for grassland and early-season herbaceous based on S2 and S3). Such increased accuracies could also be observed when classifying the late-season herbaceous community. As the community that was most widely distributed across the study area and highly mixed with all other communities, it was most intractable for classification under the default strategy (S1) with the lowest average accuracy of 82.5%. However, incorporating phenology dynamics increased the accuracy to 89.0% and 89.2% under S2 and S3.

It is clear and encouraging that the two strategies considering temporal phenological changes achieved a significant improvement on classification accuracies. Interestingly, the differences in their performances (S2 and S3) were slight or negligible for most communities and for most of the months. An exception was the tall herbaceous community in May, as it shares similar phenology (regarding the size and NDVI) with other communities by then (all at the early developing stages in the early growing season), leading to challenges in classification without summer phenology.

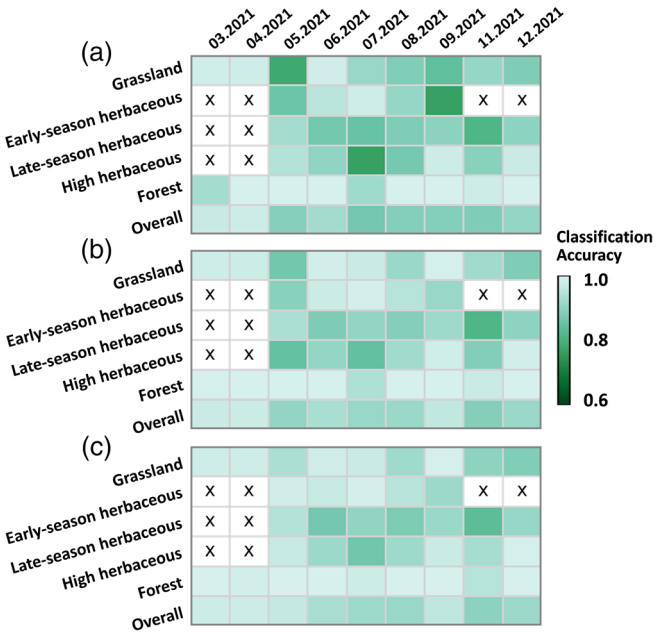

FIGURE 4 The classification accuracy for different communities based on strategy S1 (a), S2 (b), and S3 (c). White grids mean that no community was detected in that flight. "x" means the species was not detected.

3.2.2 | Feature importance

Generally, the averaged values of features within the segmented object were more important than their standard deviation (Figure 5). The only exception was the DSM, whose standard deviation also effectively contributed to the classification.

Among all the selected features, DSM and NDVI were constantly important for the classification, while the importance of other features varied significantly between flights. For instance, the band green, red edge and near-infrared exhibited higher importance in winter, while NDVI became more influential on classification in growing seasons. The texture indices showed little contribution to the classification results.

When applying data fusion for classification, the NDVI variations between flights also showed certain importance for classification. Such contribution was especially clear in the growing seasons, when communities are highly mixed. In contrast, the average value of NDVI and the date of maximum NDVI occurrence were negligible.

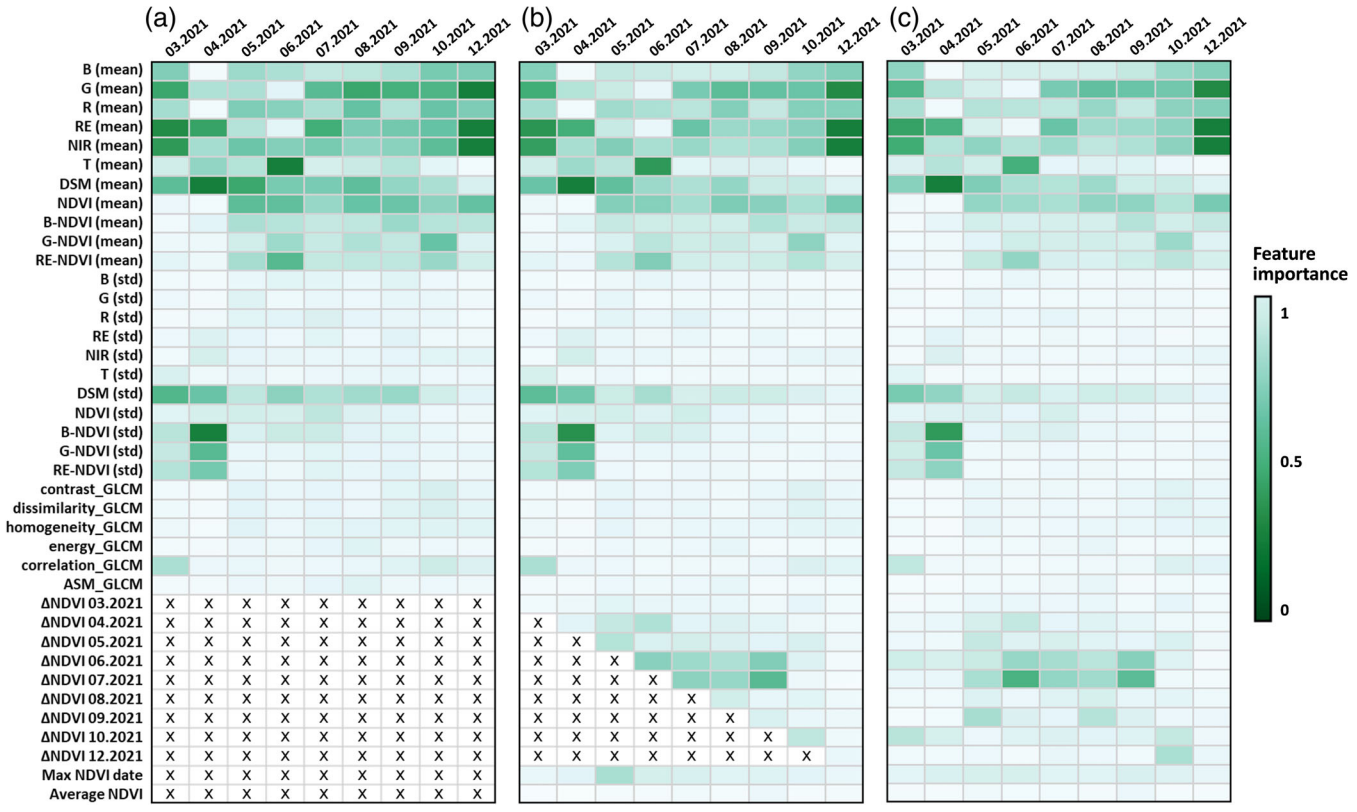

FIGURE 5 The feature importance in the monthly RF models trained based on S1 (a), S2 (b), and S3 (c). "mean" and "std" are the average values and standard deviations within an object. "x" means the feature was not included in the classification.

3.2.3 | Classification results

As shown in Figure 6, each community had its main area: early-season low herbaceous vegetation dominated the south-eastern part of the wetland; high herbaceous communities were focused in the riparian area or directly in the stream channel, while some were also distributed in a scattered manner within the southern part. The remaining riparian areas were covered by late-season low herbaceous community. Forest only accounted for a relatively small fraction of the study area – the north/east corners and edges.

From a temporal perspective, communities in the riparian wetland could not be distinguished until the beginning of the growth period in May. Interestingly, the dominating area of each community was not constant, but instead changes between communities were frequently observed as the growing season progressed. For example, in early summer the early-season low herbaceous community dominated the southern part of the wetland; however, that dominance gradually changed to the late-season low herbaceous community in late summer due to its senescence.

Such changes in community-dominance were also affected by management, specifically by mowing events. For instance, the early-season low herbaceous communities were distributed intermittently in the northern section of the wetland, however, they were replaced by late-season low herbaceous communities after the mowing event.

3.3 | Evaluating monthly NDVI variations at the ecosystem and community level

3.3.1 | Ecosystem level

From a temporal perspective, vegetation development, reflected by the increase in NDVI, started at the end of March in most areas (Figure 7). NDVI reached a maximum in early summer (around May and June) followed by a gradual decline. Management interventions also played an important role, as the vegetation development across extensive areas was reset when it was mowed and removed in June 2021 and July 2022. For instance, at the end of July 2021, the vegetation productivity remained relatively high in the northern part (mowed areas) while in unmowed southern part vegetation already senesced. Such a marked reset in development was also observed in the southern part of study area in 2022, as NDVI reached ~0.8 two months after mowing in this herbaceous-dominated area while in the remaining areas, NDVI almost dropped below 0.5. Interestingly, however, the secondary increase in NDVI of the mowed areas was relatively minor in the northern section in the drier and warmer 2022.

From a spatial perspective, NDVI was highly heterogeneous. Moreover, the spatial patterns were highly variable in time due to the different phenological developmental progress between vegetation communities and the impact from mowing events. For example, NDVI showed similar values on both sides of the downstream river in March

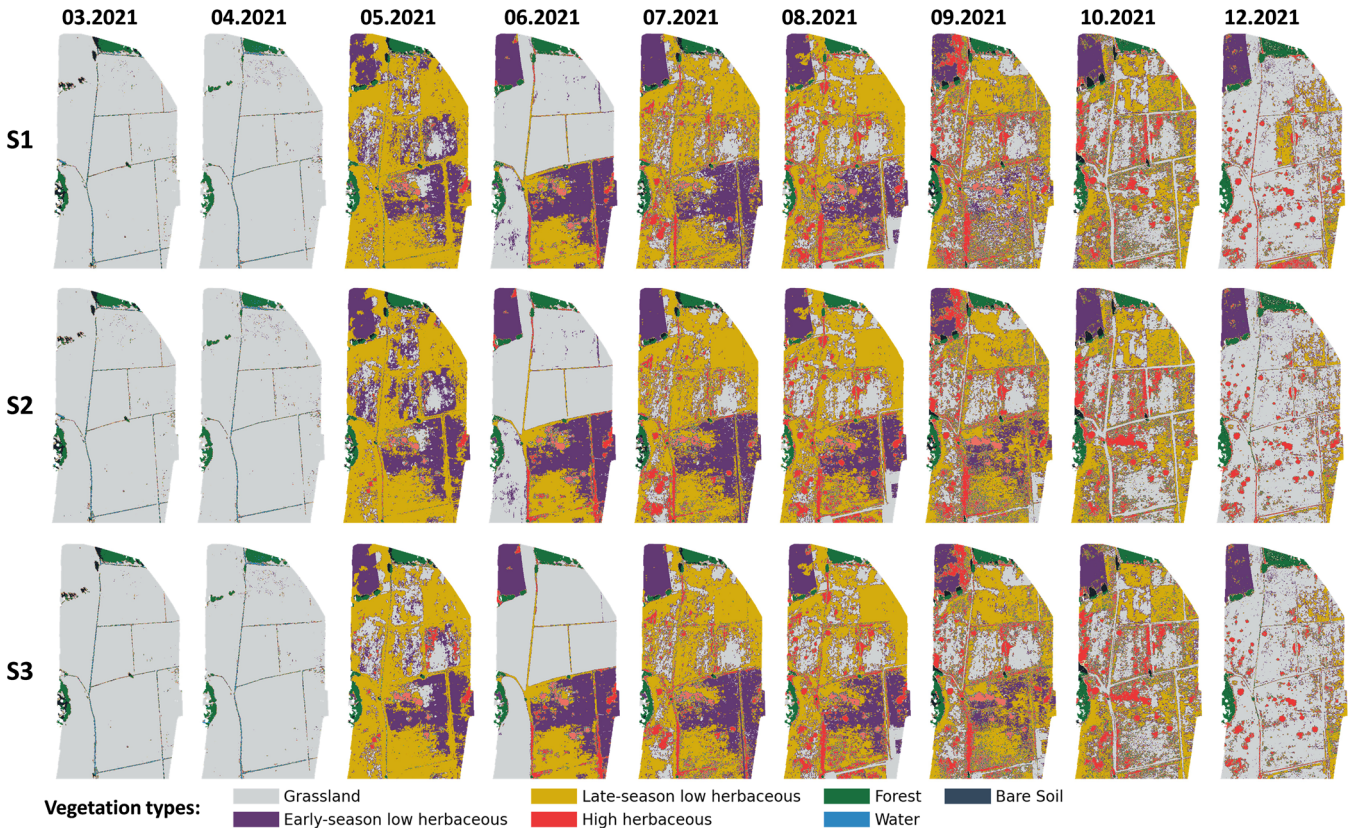

FIGURE 6 Distributions of classified vegetation communities based on three strategies (S1–S3).

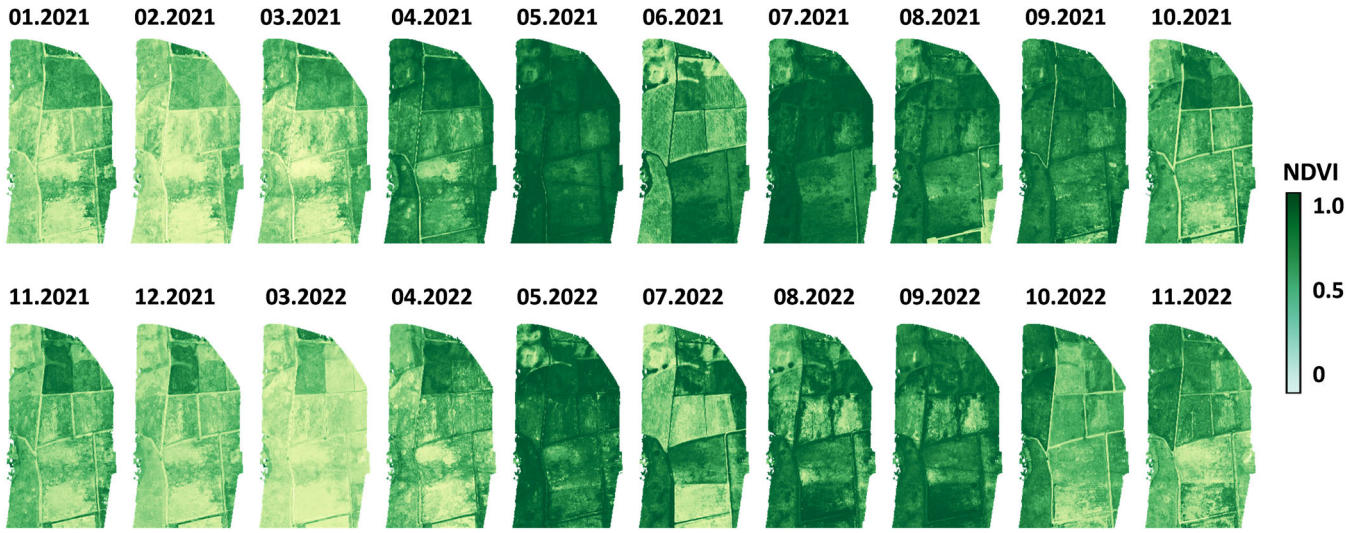

FIGURE 7 Monthly maps of NDVI.

to May 2021, but turned significantly different in July because of the mowing activity on the western riparian areas. Therefore, it is difficult to summarize any constant spatial pattern when directly looking into the monthly NDVI maps.

3.3.2 | Community level

Vegetation classification provided an opportunity to examine the dynamics of vegetation growth and development in more detail, as the temporal patterns of phenology were distinct between different communities (Figure 8). Among all the communities, the forest showed the highest NDVI over the whole year; with the greening starting in April and May, and NDVI remaining relatively high after June. The late-season low herbaceous community covered the most extensive area, and thus, their phenology was highly heterogenous. In general, plants in this community started to grow after April and flourished between May and August. Thereafter, a gradual senescence was observed. In contrast, the development and senescence of the early-season low herbaceous community (mostly in middle-east section of the wetland) were much earlier, with significant NDVI increase and decrease were already observed in March and June, respectively. The high herbaceous community development only started later in May while senescence progressed after September. This led to a relatively short maturing period (from June to August). Grassland productivity increased from April in both years and remained relatively high during May to July. The senescence was observed afterwards.

Notably, grassland responded differently to mowing in different years. In 2021, when mowing took place in June, the development of grassland was reset with an immediate recovery (shown as high NDVI values in following July, Figure 8b). However, such re-growth of the grass community was less strong with only a mild increase in NDVI after the mowing in July 2022. Such interannual differences in re-development, reflected by lower increases in NDVI after mowing events, could be also observed in early-season low herbaceous communities, while in contrast, late-season low herbaceous and high herbaceous communities showed fast recovery from mowing in both years.

3.4 | Monthly soil moisture distribution across the wetland

The volumetric moisture contents in upper soils (top 10 cm) were measured at ~30 sites each month (randomly selected each time but evenly distributed across the wetland), and showed strong spatio-temporal heterogeneity (Figure 9a). From a temporal perspective, the lowest moisture contents (down to <20%) were observed in summer from end of June to September, while in winter the moisture could reach above 50%. Soil moisture was spatially highly variable and no general patterns could be summarized, for example, the moisture in the NE section was lower than the SE section in March 2021 but an opposite pattern was found in June, September, and August. However, more insights wwere available when incorporating the classification results (Figure 9b), as the moisture content was generally negatively related to the NDVI of the local community, and lowest soil moisture was usually observed during NDVI peaks. The inter-community differences were also marked, given moisture content was similar between areas dominated by three herbaceous community while the lowest moisture contents were always found under grassland.

4 | DISCUSSION

4.1 | Advances of multi-flight-based classification

Vegetation classification has always been a useful tool to aid land management (Belgiu & Drăgu, 2016; Xie et al., 2008), especially considering the modern UAV technologies that provide imagery with ultra-high resolution (Candiago et al., 2015; Yeom et al., 2019).

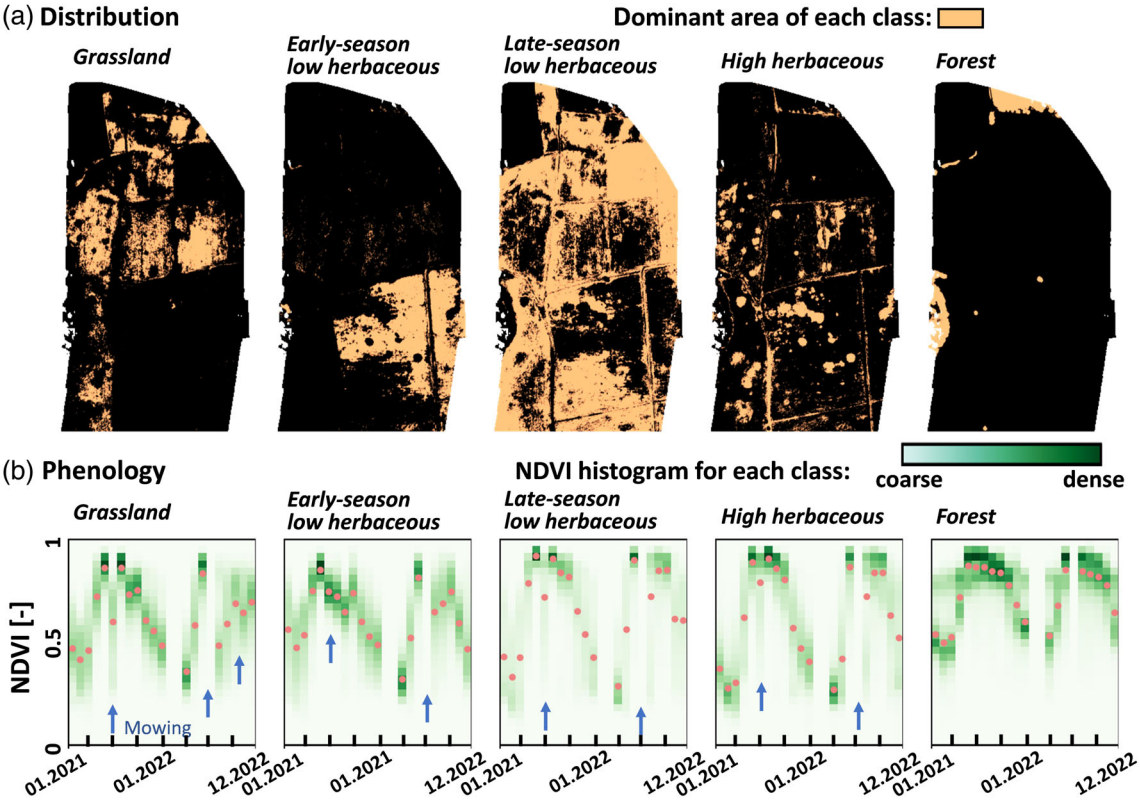

FIGURE 8 (a) The distribution of major communities. (b) The phenology of each community summarized as NDVI histogram in their dominant area. The dates of mowing events are shown as blue arrows. Red dotes denote the median values.

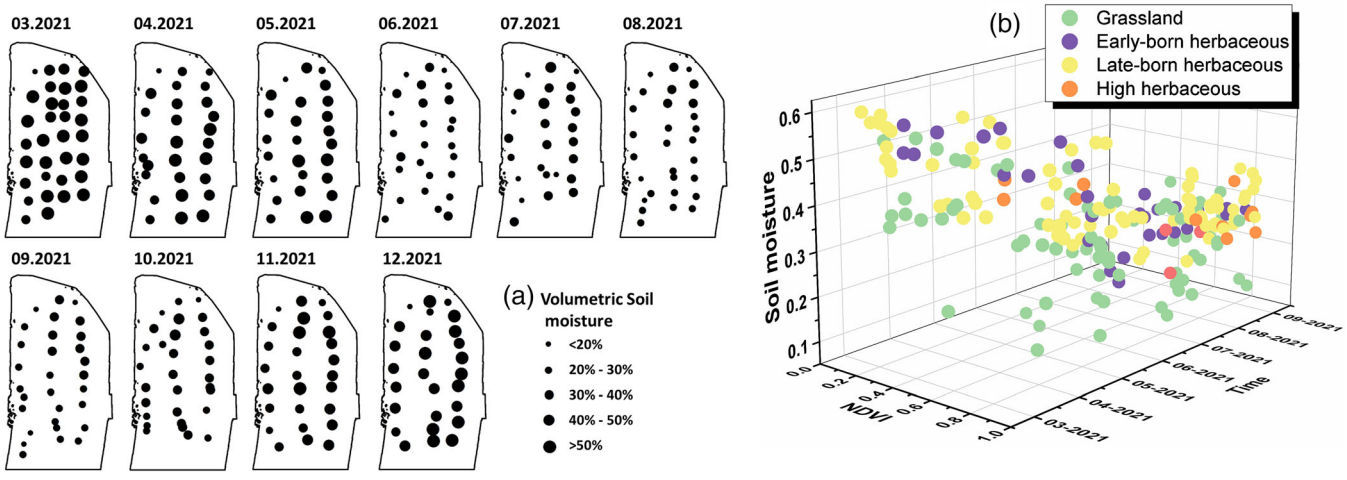

FIGURE 9 Upper soil moisture contents (top 10 cm; a) and their relationships with vegetation distribution (b).

However, though benefiting from finer resolutions, the classification in grass-dominated areas is still often problematic, as those grass or herbaceous species and communities are generally small in size and highly mixed. But its hydrological important areas such as wetlands that are often characterized by these complex vegetation communities. Here, to address this issue, unique monthly UAV imagery was collected for two years for vegetation classification at the community level in a managed wetland to improve understanding of vegetation-water interlinakges. Such datasets with relatively long duration and monthly resolution have been, to authors' knowledge, rarely used for vegetation classification in wetlands (though there are several studies in grasslands based on multi-seasonal flights but with less temporal frequency, e.g., Bendig et al., 2014 and van Iersel et al., 2018). Such studies are very informative for evaluating multi-flight-based classification against traditional single-flight-based applications, and helping guide the development of optimal strategies for UAV surveys that balance time and resource availability against the degree of accuracy required.

Like many previous studies (e.g., Dumont et al., 2012; Marion et al., 2010), the classification was not ideal when starting with datasets from a single flight. Our application based on S1 achieved an acceptable overall accuracy, it included some classes that are very distinct from grass/herbaceous communities and thus, can be always successfully distinguished (e.g., forest and open water). In contrast,, the accuracies of grass or herbaceous communities could sometimes drop to <60%, especially in early summer when most vegetations were developing. Such difficulties in discrimination have also been found in other applications (e.g., Bradter et al., 2019), as fully developed vegetation canopies can result in mixed spectra within or between communities and thus impede precise classification. Multi-flight-based classification clearly performs better when spectra information from a single flight is not sufficient to distinguish these small-sized grass/herbaceous communities. By incorporating the NVDI variations between flights, the model was now informed by not only the current spectra information in each segmented object across the wetland, but also *where* and *when* different vegetation started to develop in that object, and *how* that development progressed through time. Assisted with such axillary "historical" information, those mixed communities could be better distinguished with higher accuracy. Moreover, multiple-flight-based application could potentially reduce the impacts from radiometric uncertainties, which are almost unavoidable in UAV applications. Although the reflectance maps were iteratively calibrated against different radiometric references (to exclude the ones producing abnormal results), it is likely that the selected reference for calibration could not entirely cover the weather conditions throughout the flight but additional information from multi-temporal flights apparently reduced the risk of distorted radiometry.

Multi-flight-based classifications bring also benefits from an ecological perspective. When mapping vegetation at community level throughout an entire growing season, the evolution between different communities and their changing distributions become much clearer. Multiple flights (particular spanning over several seasons) could provide a more comprehensive picture of vegetation change over the year (in the form of dynamic boundaries of each community acquired from monthly classification results) than single flights.

Despite multi-flight-based classifications providing more robust results with higher accuracy, monthly UAV flights are still rare as resources for data acquisition are usually limited, and remote sensing is often meant to be used for data scarce regions (Nordberg & Evertson, 2005). Therefore, it is key to identify optimal strategies for classification-oriented UAV surveys for wetland or grassland management, which aim for more informative and robust vegetation data from as few flights as possible.

From inspection of the monthly vegetation distributions, the main communities were observed in most classifications during the growing season (Figure 6). The main differences between these months were the gradual changes from early-season herbaceous to late-season herbaceous communities in early summer (end of May) and the change from late-season herbaceous community to grass in late summer (at the end of September and October). A full picture of vegetation distribution could likely be adequately summarized from only a few flights, at the beginning of the growing season, in early summer and late summer, respectively. This is of course site-dependent, but can be informative for many regions sharing a similar climatic background (e.g., temperate grasslands or wetlands across the extensive Northern European Plain). Similar conclusions were also reached for woody or forest communities with only three optimal time steps, mostly in early and late summer (Michez et al., 2016; van Iersel et al., 2018; Weil et al., 2017). However, in the case that only one flight is scheduled within a year, mid-summer (June or July in the northern hemisphere) would be a more appropriate timing, as most communities are fully developed and exert relatively strong impacts on the ecohydrology by then, compared to spring (late-season herbaceous community is still developing) or late summer (when early-season herbaceous community already starts to senesce).

4.2 | Improved mapping of vegetation dynamics via community-level analysis

The initial goal of this study was to characterize the vegetation development in a riparian wetland. However, we found it challenging to directly analyse the VIs derived from UAV imagery in our wetland because of the extreme spatial heterogeneity captured by the fine-resolution sensor (Bradter et al., 2019). Such complexity was further amplified when the boundaries between the dominant areas of each community changed through time, making it almost impossible to directly interpret the spatio-temporal pattern of VIs, though time series of NDVI are available for almost two years (Figure 7). In this context, vegetation classification helped as it allowed downscaling of the VI analysis to a realistic community level (Geerling et al., 2007), providing invaluable information on not only the spatial distribution of each community across the wetland, but also how their development changed temporally (Section 3.3.2).

Another important finding is related to how vegetation responded differently to management disturbances through mowing for hay production. We found different responses of grassland and early-season low herbaceous communities to the major mowing events in two years. their re-developments were marked with an immediate recovery (shown as relatively high NDVI value in the following month) in 2021 but being damped with only a mild increase in NDVI after the mowing in July 2022. This, could be either attributed to the dry and warmer conditions in 2022, as re-developments of these communities need certain degrees of soil moisture for root water uptake (Dumont et al., 2012); or to the timing of management as the mowing was conducted in different months (June in 2021; July in 2022). The suppressed recovery in 2022 suggests that the vegetation resilience to anthropogenic activities was also related to *when* that activity took place and at *which* development stage the communities were at that moment. This further emphasizes the importance of an appropriate timing when applying management practices in wetlands, because management interventions during later development stages may result in an abrupt senescence of specific vegetation communities (e.g., grass or early-season herbaceous in our wetland). However, the inter-annual differences in recovery were not observed in the late-season low herbaceous and high herbaceous as they both showed a

strong recovery from mowing. It seems that grass and early-season herbaceous communities are more vulnerable to external pressures, as their development could be strongly affected or even truncated by mowing activities in mid-summer while other communities could still effectively recover. Of course, such conclusions are only based on NDVI values in two years, which could be different from a long-term perspective or in another ecosystem.

These detailed insights brought by community-level analysis provided not only a solid evidence-base for wetland management, but also a starting point for stronger interdisciplinary research using remote sensing techniques as vegetation is fundamental to almost all wetland ecosystem services and functions.

4.3 | Wider implication for ecohydrology

The interdependent relationship between vegetation and hydrology has long recognized that plants naturally rely on water availability, while also contributing to the water cycle via interception and transpiration (Chapin et al., 2011; Tabacchi et al., 2000; Tetzlaff et al., 2021). Measurements of hydrological fluxes at local scales help to infer interesting and integrated insights into vegetation-water interactions.

We measured the moisture content of the upper soil layer (10 cm) during each flight at ~30 sites across the wetland (Figure 9a), and tested its relationship with the local vegetation communities and NDVI (Figure 9b). Maximum vegetation development was usually observed during periods of minimum values of soil moisture, mostly when the NDVI of the local vegetation community peaked. This reflects the close relationship between vegetation development and the evolution of soil moisture deficits, which are consistent with higher transpiration in summer (Smith et al., 2021). Without such detailed UAV-based mapping, we would have been unable to explain why the strongest deficit of soil moisture was observed at different months under early-season and late-season low herbaceous communities, given that these sites share very similar soil properties and hydroclimatic characteristics.

Moreover, when considering inter-community differences, lower moisture contents were mainly observed under grassland, especially for those occasions when soil moisture fell below 20% (Figure 9b). Given that the grass in our wetland is small in size and with less dense distribution compared to the herbaceous communities, the water deficit is unlikely attributed to the high transpiration rates (though soil evaporation could increase due to coarser vegetation cover). One reason for the low moisture contents under grassland could be the ground elevationas the grass communities are more present on "elevated" areas across the wetland (though the elevations of those prominence are only slightly higher by <0.5 m than their surroundings). Considering the groundwater table is flat (spatially) and relatively stable (temporally) in this area (see groundwater level at three wells across the wetland since 2015 in Figure S1), such variations in ground elevation could be sufficient to cause accentuated water deficits in the upper soil layer and limit vegetation uptake (Scheliga et al., 2019). Thus, the vegetation communities are not a driver of variable hydrological states/fluxes, but instead their distributions are an integrated result of local hydrological conditions and topography.

Such improved understanding of water-vegetation relationships can assist the prediction of soil moisture using statistical or machine learning models, as previous applications based on fine resolution imagery often met challenges due to the lack of fine-resolution input features that were able to interpret the extreme spatial heterogeneity in soil moisture (e.g., Araya et al., 2021; Zaman et al., 2012). Given the bidirectional relationships observed in our wetland, vegetation classification and the following species-level analysis of VIs can potentially help the direct prediction of soil moisture distribution, which is a planned next step in research at the study site.

Finally, the detailed vegetation mapping is also informative for process-based hydrological modelling (besides being directly used to analyse or predict the hydrological observations via data-driven models), given vegetation functioning is a fundamental compartment in almost every ecohydrological model (Wellen et al., 2015). Knowledge about the community distribution and its developmental progress can certainly improve the conceptualisation of interception and transpiration at finer spatial and temporal scales. The spatial distribution of different vegetation communities also provides an evidence base for the parameterisation of distributed modelling, which significantly reduces the computation burden and parametric uncertainty, while retaining a comparable representation of the spatial heterogeneity (Herman et al., 2013; Werkhoven et al., 2008; Wu, Tetzlaff, Yang, & Soulsby, 2022). For instance, the mapping acquired from this study has been used in recent modelling in this area via a physics-based, fully distributed ecohydrological model EcH$_2$O-iso. With such detailed vegetation conceptualisation, the model managed to capture the spatio-temporal patterns of multiple hydrological indices (e.g., discharge, stream isotopes, groundwater isotopes, and soil moisture at distributed sites) with internal flux simulations also being physically realistic (Wu et al., submitted). Such an interdisciplinary fusion of field and remote sensing ecohydrological data with ecohydrological modelling has many advantages given the well-known challenges often arising for distributed modelling to capture full spatial heterogeneity in ecohydrological function (Beven & Freer, 2001; Wellen et al., 2015). These challenges are, of course, related to errors and uncertainties in model structure or measurements, but can also be linked to the coarse conceptualisation of spatial inputs and outputs in which vegetation plays a key role in partitioning.

5 | CONCLUSION

In this study, monthly UAV surveys were conducted over two years in a riparian wetland in north-eastern Germany, with collected imagery used for vegetation classification on a monthly basis. Different strategies were tested for classification, that is, respectively using imagery from the current survey (S1), from the current and the previous surveys (S2), and from all surveys (S3).

The results show that multi-flight-based classification (S2 and S3) outperformed single-flight-based classification (S1) due to the higher classification accuracy (though the performances of S2 and S3 were similarly good). Moreover, we observed marked temporal changes in the boundaries of community distributions according to the classified

maps, which highlights the benefits of multi-flight-based classification - providing a more comprehensive picture of intra- and inter-annual vegetation community evolution. After checking the performance of classification applications, we further suggest that a combination of two or three flights in early- and late-summer would be enough to achieve comparable results to monthly flights, while mid-summer would be the best timing in case only one flight is possible.

With such detailed information from monthly vegetation mapping, the complex spatio-temporal heterogeneity in NDVI could be, to a certain extent, interpreted by community distribution and evolution. Moreover, we evaluated the impacts of management interventions such as mowing events based on the different responses between communities, which were mainly attributed to the inherent characteristics of the community (less resilience for grass and early-season herbaceous), the timing of management (early or late summer), and the wetness condition (drier and warmer conditions in 2022). We also could summarize the dominant areas and developmental progress of each community.

Finally, we explored how such vegetation mapping could help understand landscape ecohydrology, and found the spatio-temporal distribution of minimal soil moisture was related to NDVI peaks of the local community and grass distribution could be interpreted by topography and low moisture conditions. Such bidirectional relationships proved that apart from the direct evidence base for wetland management, multi-flight-based vegetation mapping could also help improve understanding on landscape ecohydrology providing a fundamental prerequisite for further interdisciplinary research and parametrisation of process-based models.

ACKNOWLEDGEMENTS

Songjun Wu was funded by the Chinese Scholarship Council (CSC). Tetzlaff's contribution was partly funded through the Einstein Research Unit "Climate and Water under Change" from the Einstein Foundation Berlin and Berlin University Alliance (grant no. ERU-2020-609). Contributions from Soulsby were supported by the Leverhulme Trust through the ISO-LAND project (grant no. RPG 2018 375). We also thank colleagues from the Finck Foundation (www.finck-stiftung.org) Benedict Boesel and Max Kuester for the trustful collaboration and for providing access to the study sites. Open Access funding enabled and organized by Projekt DEAL.

DATA AVAILABILITY STATEMENT

The data that support the findings of this study are available from the corresponding author upon reasonable request.

ORCID

Songjun Wu https://orcid.org/0000-0003-1758-5714
Chris Soulsby https://orcid.org/0000-0001-6910-2118

REFERENCES

Ahmed, O. S., Shemrock, A., Chabot, D., Dillon, C., Williams, G., Wasson, R., & Franklin, S. E. (2017). Hierarchical land cover and vegetation classification using multispectral data acquired from an unmanned aerial vehicle. *International Journal of Remote Sensing*, *38*, 2037–2052. https://doi.org/10.1080/01431161.2017.1294781

Andrew, M. E., & Ustin, S. L. (2008). The role of environmental context in mapping invasive plants with hyperspectral image data. *Remote Sensing of Environment*, *112*, 4301–4317. https://doi.org/10.1016/J.RSE.2008.07.016

Araya, S. N., Fryjoff-Hung, A., Anderson, A., Viers, J. H., & Ghezzehei, T. A. (2021). Advances in soil moisture retrieval from multispectral remote sensing using unoccupied aircraft systems and machine learning techniques. *Hydrology and Earth System Sciences*, *25*, 2739–2758. https://doi.org/10.5194/HESS-25-2739-2021

Asrar, G., Fuchs, M., Kanemasu, E. T., & Hatfield, J. L. (1984). Estimating absorbed photosynthetic radiation and leaf area index from spectral reflectance in wheat 1. *Agronomy Journal*, *76*, 300–306. https://doi.org/10.2134/AGRONJ1984.00021962007600020029X

Astor, T., Dalmayne, J., Prentice, H. C., Eklundh, L., Purschke, O., Schmidtlein, S., & Hall, K. (2014). Classification of grassland successional stages using airborne hyperspectral imagery. *Remote Sensing*, *6*, 7732–7761. https://doi.org/10.3390/RS6087732

Baron, J., & Hill, D. J. (2020). Monitoring grassland invasion by spotted knapweed (Centaurea maculosa) with RPAS-acquired multispectral imagery. *Remote Sensing of Environment*, *249*, 112008. https://doi.org/10.1016/J.RSE.2020.112008

Belgiu, M., & Drăgu, L. (2016). Random forest in remote sensing: A review of applications and future directions. *ISPRS Journal of Photogrammetry and Remote Sensing*, *114*, 24–31. https://doi.org/10.1016/J.ISPRSJPRS.2016.01.011

Bendig, J., Bolten, A., Bennertz, S., Broscheit, J., Eichfuss, S., & Bareth, G. (2014). Estimating biomass of barley using crop surface models (CSMs) derived from UAV-based RGB imaging. *Remote Sensing*, *6*, 10395–10412. https://doi.org/10.3390/RS61110395

Beven, K., & Freer, J. (2001). Equifinality, data assimilation, and uncertainty estimation in mechanistic modelling of complex environmental systems using the GLUE methodology. *Journal of Hydrology*, *249*, 11–29. https://doi.org/10.1016/S0022-1694(01)00421-8

Bradter, U., O Connell, J., Kunin, W., Boffey, C. W. H., Ellis, R., & Benton, T. (2019). Classifying grass-dominated habitats from remotely sensed data: The influence of spectral resolution, acquisition time and the vegetation classification system on accuracy and thematic resolution. *Science of the Total Environment*, *711*, 134584. https://doi.org/10.1016/j.scitotenv.2019.134584

Bunting, P., Clewley, D., Lucas, R. M., & Gillingham, S. (2014). The remote sensing and GIS software library (RSGISLib). *Computational Geosciences*, *62*, 216–226. https://doi.org/10.1016/J.CAGEO.2013.08.007

Candiago, S., Remondino, F., de Giglio, M., Dubbini, M., & Gattelli, M. (2015). Evaluating multispectral images and vegetation indices for precision farming applications from UAV images. *Remote Sensing*, *7*, 4026–4047. https://doi.org/10.3390/RS70404026

Chapin, F. S., Matson, P. A., & Vitousek, P. M. (2011). Landscape heterogeneity and ecosystem dynamics. In *Principles of terrestrial ecosystem ecology* (pp. 369–397). Springer. https://doi.org/10.1007/978-1-4419-9504-9_13

Cole, E., & Sheldon, B. (2017). The shifting phenological landscape: Within- and between-species variation in leaf emergence in a mixed-deciduous woodland. *Ecology and Evolution*, *7*, 1135–1147. https://doi.org/10.1002/ece3.2718

Dirnböck, T., Dullinger, S., Gottfried, M., Ginzier, C., & Grabherr, G. (2003). Mapping alpine vegetation based on image analysis, topographic variables and canonical correspondence analysis. *Applied Vegetation Science*, *6*, 85–96. https://doi.org/10.1111/J.1654-109X.2003.TB00567.X

Donaldson, J., & Lindroth, R. (2008). Effects of variable phytochemistry and budbreak phenology on defoliation of aspen during a forest tent caterpillar outbreak. *Agricultural and Forest Entomology*, *10*, 399–410. https://doi.org/10.1111/j.1461-9563.2008.00392.x

Dumont, B., Rossignol, N., Loucougaray, G., Carrère, P., Chadoeuf, J., Fleurance, G., Bonis, A., Farruggia, A., Gaucherand, S., Ginane, C., Louault, F., Marion, B., Mesléard, F., & Yavercovski, N. (2012). When

does grazing generate stable vegetation patterns in temperate pastures? *Agriculture, Ecosystems and Environment*, *153*, 50–56. https://doi.org/10.1016/j.agee.2012.03.003

Feilhauer, H., & Schmidtlein, S. (2011). On variable relations between vegetation patterns and canopy reflectance. *Ecological Informatics*, *6*, 83–92. https://doi.org/10.1016/j.ecoinf.2010.12.004

Geerling, G., Labrador García, M., Clevers, J. G. P. W., Ragas, A. M. J., & Smits, A. J. M. (2007). Classification of floodplain vegetation by data fusion of spectral (CASI) and LiDAR data. *International Journal of Remote Sensing*, *28*, 19–28. https://doi.org/10.1080/01431160701241720

Hamylton, S. M., Morris, R. H., Carvalho, R., Roder, N., Barlow, P., Mills, K., & Wang, L. (2020). Evaluating techniques for mapping Island vegetation from unmanned aerial vehicle (UAV) images: Pixel classification, visual interpretation and machine learning approaches. *International Journal of Applied Earth Observation and Geoinformation*, *89*, 102085. https://doi.org/10.1016/j.jag.2020.102085

Herman, J. D., Kollat, J. B., Reed, P. M., & Wagener, T. (2013). From maps to movies: High-resolution time-varying sensitivity analysis for spatially distributed watershed models. *Hydrology and Earth System Sciences*, *17*(12), 5109–5125. https://doi.org/10.5194/HESS-17-5109-2013

Kariyeva, J., & van Leeuwen, W. J. D. (2011). Environmental drivers of NDVI-based vegetation phenology in Central Asia. *Remote Sensing*, *3*, 203–246. https://doi.org/10.3390/RS3020203

Komarek, J., Klouček, T., & Prošek, J. (2018). The potential of unmanned aerial systems: A tool towards precision classification of hard-to-distinguish vegetation types? *International Journal of Applied Earth Observation and Geoinformation*, *71*, 9–19. https://doi.org/10.1016/j.jag.2018.05.003

Kumar, L., & Sinha, P. (2014). Mapping salt-marsh land-cover vegetation using high-spatial and hyperspectral satellite data to assist wetland inventory. *GIScience & Remote Sensing*, *51*, 1–16. https://doi.org/10.1080/15481603.2014.947838

Laba, M., Tsai, F., Ogurcak, D., Smith, S., & Richmond, M. E. (2005). Field determination of optimal dates for the discrimination of invasive wetland plant species using derivative spectral analysis. *Photogrammetric Engineering and Remote Sensing*, *71*, 603–611. https://doi.org/10.14358/PERS.71.5.603

Laliberte, A., Goforth, M., Steele, C., & Rango, A. (2011). Multispectral remote sensing from unmanned aircraft: Image processing workflows and applications for rangeland environments. *Remote Sensing*, *3*(11), 2529–2551. https://doi.org/10.3390/rs3112529

Laliberte, A., & Rango, A. (2011). Image processing and classification procedures for analysis of sub-decimeter imagery acquired with an unmanned aircraft over arid rangelands. *GIScience & Remote Sensing*, *48*, 4–23. https://doi.org/10.2747/1548-1603.48.1.4

Laliberte, A., Winters, C., & Rango, A. (2011). UAS remote sensing missions for rangeland applications. *Geocarto International*, *26*, 141–156. https://doi.org/10.1080/10106049.2010.534557

Laliberte, A. S., & Rango, A. (2009). Texture and scale in object-based analysis of subdecimeter resolution unmanned aerial vehicle (UAV) imagery. *IEEE Transactions on Geoscience and Remote Sensing*, *47*, 761–770. https://doi.org/10.1109/TGRS.2008.2009355

López-Granados, F., Torres-Sánchez, J., Serrano-Pérez, A., de Castro, A., Mesas-Carrascosa, F., & Peña-Barragán, J. M. (2016). Early season weed mapping in sunflower using UAV technology: Variability of herbicide treatment maps against weed thresholds. *Precision Agriculture*, *17*, 183–199. https://doi.org/10.1007/s11119-015-9415-8

Lu, B., & He, Y. (2017). Species classification using unmanned aerial vehicle (UAV)-acquired high spatial resolution imagery in a heterogeneous grassland. *ISPRS Journal of Photogrammetry and Remote Sensing*, *128*, 73–85. https://doi.org/10.1016/j.isprsjprs.2017.03.011

Marion, B., Bonis, A., & Bouzillé, J.-B. (2010). How much does grazing-induced heterogeneity impact plant diversity in wet grasslands? *Ecoscience*, *17*, 229–239. https://doi.org/10.2980/17-3-3315

Martínez-López, J., Carreño, M., Palazón-Ferrando, J. A., Martínez-Fernández, J., & Esteve-Selma, M. A. (2014). Remote sensing of plant communities as a tool for assessing the condition of semiarid Mediterranean saline wetlands in agricultural catchments. *International Journal of Applied Earth Observation and Geoinformation*, *26*, 193–204. https://doi.org/10.1016/j.jag.2013.07.005

McQueen, J. (1967). Some methods for classification and analysis of multivariate observations. *Computers & Chemistry*, *4*, 257–272.

Michez, A., Piégay, H., Lisein, J., Claessens, H., & Lejeune, P. (2016). Classification of riparian forest species and health condition using multi-temporal and hyperspatial imagery from unmanned aerial system. *Environmental Monitoring and Assessment*, *188*, 1–19. https://doi.org/10.1007/S10661-015-4996-2

Modica, G., de Luca, G., Messina, G., & Praticò, S. (2021). Comparison and assessment of different object-based classifications using machine learning algorithms and UAVs multispectral imagery: A case study in a citrus orchard and an onion crop. *European Journal of Remote Sensing*, *54*, 431–460. https://doi.org/10.1080/22797254.2021.1951623

Müllerová, J., Brůna, J., Bartaloš, T., Dvořák, P., Vítková, M., & Pyšek, P. (2017). Timing is important: Unmanned aircraft vs. satellite imagery in plant invasion monitoring. *Frontiers in Plant Science*, *8*, 1–13. https://doi.org/10.3389/fpls.2017.00887

Nemani, R. R., Keeling, C. D., Hashimoto, H., Jolly, W. M., Piper, S. C., Tucker, C. J., Myneni, R. B., & Running, S. W. (2003). Climate-driven increases in global terrestrial net primary production from 1982 to 1999. *Science (1979)*, *300*, 1560–1563. https://doi.org/10.1126/SCIENCE.1082750

Nordberg, M. L., & Evertson, J. (2005). Vegetation index differencing and linear regression for change detection in a Swedish mountain range using Landsat TM® and ETM+® imagery. *Land Degradation and Development*, *16*, 139–149. https://doi.org/10.1002/LDR.660

Pal, M. (2005). Random forest classifier for remote sensing classification. *International Journal of Remote Sensing*, *26*, 217–222. https://doi.org/10.1080/01431160412331269698

Palace, M., Herrick, C., DelGreco, J., Finnell, D., Garnello, A., Mccalley, C., McArthur, K., Sullivan, F., & Varner, R. (2018). Determining subarctic peatland vegetation using an unmanned aerial system (UAS). *Remote Sensing*, *10*, 1498. https://doi.org/10.3390/rs10091498

Pande-Chhetri, R., Abd-Elrahman, A., Liu, T., Morton, J., & Wilhelm, V. (2017). Object-based classification of wetland vegetation using very high-resolution unmanned air system imagery. *European Journal of Remote Sensing*, *50*, 564–576. https://doi.org/10.1080/22797254.2017.1373602

Penman, H. (1948). Natural evaporation from open water, bare soil and grass. *Proceedings of the Royal Society A: Mathematical, Physical and Engineering Sciences*, *193*, 120–145. https://doi.org/10.1098/rspa.1948.0037

Pettorelli, N., Vik, J. O., Mysterud, A., Gaillard, J. M., Tucker, C. J., & Stenseth, N. C. (2005). Using the satellite-derived NDVI to assess ecological responses to environmental change. *Trends in Ecology & Evolution*, *20*, 503–510. https://doi.org/10.1016/J.TREE.2005.05.011

Pottier, J., Malenovský, Z., Psomas, A., Homolova, L., Schaepman, M., Choler, P., Thuiller, W., Guisan, A., & Zimmermann, N. (2014). Modelling plant species distribution in alpine grasslands using airborne imaging spectroscopy. *Biology Letters*, *10*, 20140347. https://doi.org/10.1098/rsbl.2014.0347

Rapinel, S., Mony, C., Lecoq, L., Clement, B., Thomas, A., & Hubert-Moy, L. (2019). Evaluation of Sentinel-2 time-series for mapping floodplain grassland plant communities. *Remote Sensing of Environment*, *223*, 115–129. https://doi.org/10.1016/j.rse.2019.01.018

Roth, K., Roberts, D., Dennison, P., Peterson, S., & Alonzo, M. (2015). The impact of spatial resolution on the classification of plant species and functional types within imaging spectrometer data. *Remote Sensing of Environment*, *171*, 45–57. https://doi.org/10.1016/j.rse.2015.10.004

Scheliga, B., Tetzlaff, D., Nuetzmann, G., & Soulsby, C. (2019). Assessing runoff generation in riparian wetlands: Monitoring groundwater–

surface water dynamics at the micro-catchment scale. *Environmental Monitoring and Assessment*, *191*, 116. https://doi.org/10.1007/S10661-019-7237-2

Schonberger, J. L., & Frahm, J. M. (2016). Structure-from-motion revisited. In *Proceedings of the IEEE computer society conference on computer vision and pattern recognition* (pp. 4104–4113). Las Vegas, NV. https://doi.org/10.1109/CVPR.2016.445

Sellers, P. J., Berry, J. A., Collatz, G. J., Field, C. B., & Hall, F. G. (1992). Canopy reflectance, photosynthesis, and transpiration. III. A reanalysis using improved leaf models and a new canopy integration scheme. *Remote Sensing of Environment*, *42*, 187–216. https://doi.org/10.1016/0034-4257(92)90102-P

Senf, C., Leitão, P. J., Pflugmacher, D., van der Linden, S., & Hostert, P. (2015). Mapping land cover in complex Mediterranean landscapes using Landsat: Improved classification accuracies from integrating multi-seasonal and synthetic imagery. *Remote Sensing of Environment*, *156*, 527–536. https://doi.org/10.1016/J.RSE.2014.10.018

Shepherd, J., Bunting, P., & Dymond, J. (2019). Operational large-scale segmentation of imagery based on iterative elimination. *Remote Sensing*, *11*, 658. https://doi.org/10.3390/rs11060658

Smith, A., Tetzlaff, D., Kleine, L., Maneta, M., & Soulsby, C. (2021). Quantifying the effects of land use and model scale on water partitioning and water ages using tracer-aided ecohydrological models. *Hydrology and Earth System Sciences*, *25*, 2239–2259. https://doi.org/10.5194/HESS-25-2239-2021

Son, N. T., Chen, C. F., Chen, C. R., Duc, H. N., & Chang, L. Y. (2013). A phenology-based classification of time-series MODIS data for rice crop monitoring in Mekong Delta, Vietnam. *Remote Sensing (Basel)*, *6*, 135–156. https://doi.org/10.3390/RS6010135

Tabacchi, E., Lambs, L., Guilloy, H., Planty-Tabacchi, A.-M., Muller, E., & Decamps, H. (2000). Impacts of riparian vegetation on hydrological processes. *Hydrological Processes*, *14*, 2959–2976. https://doi.org/10.1002/1099-1085(200011/12)14:16/173.3.CO;2-2

Tetzlaff, D., Buttle, J., Carey, S. K., Kohn, M. J., Laudon, H., McNamara, J. P., Smith, A., Sprenger, M., & Soulsby, C. (2021). Stable isotopes of water reveal differences in plant – Soil water relationships across northern environments. *Hydrological Processes*, *35*, e14023. https://doi.org/10.1002/HYP.14023

van Iersel, W., Straatsma, M., Middelkoop, H., & Addink, E. (2018). Multitemporal classification of river floodplain vegetation using time series of UAV images. *Remote Sensing*, *10*, 1144. https://doi.org/10.3390/rs10071144

Wang, C., Hunt, E. R., Zhang, L., & Guo, H. (2013). Phenology-assisted classification of C3 and C4 grasses in the U.S. Great Plains and their climate dependency with MODIS time series. *Remote Sensing of Environment*, *138*, 90–101. https://doi.org/10.1016/J.RSE.2013.07.025

Wang, H., Dong, H., Mu, Y., Jiang, L., Yao, X., Bai, Y., Lu, Q., & Wang, F. (2019). Landscape-level vegetation classification and fractional woody and herbaceous vegetation cover estimation over the dryland ecosystems by unmanned aerial vehicle platform. *Agricultural and Forest Meteorology*, *278*, 107665. https://doi.org/10.1016/j.agrformet.2019.107665

Weil, G., Lensky, I., Resheff, Y., & Levin, N. (2017). Optimizing the timing of unmanned aerial vehicle image Acquisition for Applied Mapping of Woody vegetation species using feature selection. *Remote Sensing*, *9*, 1130. https://doi.org/10.3390/rs9111130

Weisberg, P., Dilts, T., Greenberg, J., Johnson, K., Pai, H., Sladek, C., et al. (2021). Phenology-based classification of invasive annual grasses to the species level. *Remote Sensing of Environment*, *263*, 112568. https://doi.org/10.1016/j.rse.2021.112568

Wellen, C., Kamran-Disfani, A. R., & Arhonditsis, G. B. (2015). Evaluation of the current state of distributed watershed nutrient water quality modeling. *Environmental Science & Technology*, *49*, 3278–3290. https://doi.org/10.1021/ES5049557

Werkhoven, K., Wagener, T., Reed, P., & Yong, T. (2008). Rainfall characteristics define the value of streamflow observations for distributed watershed model identification. *Geophysical Research Letters*, *35*, L11403. https://doi.org/10.1029/2008GL034162

Wu, C., Peng, D., Soudani, K., Siebicke, L., Gough, C. M., Arain, M. A., Bohrer, G., Lafleur, P. M., Peichl, M., Gonsamo, A., Xu, S., Fang, B., & Ge, Q. (2017). Land surface phenology derived from normalized difference vegetation index (NDVI) at global FLUXNET sites. *Agricultural and Forest Meteorology*, *233*, 171–182. https://doi.org/10.1016/J.AGRFORMET.2016.11.193

Wu, S., Tetzlaff, D., Goldhammer, T., Freymueller, J., & Soulsby, C. (2022). Tracer-aided identification of hydrological and biogeochemical controls on in-stream water quality in a riparian wetland. *Water Research*, *222*, 118860. https://doi.org/10.1016/J.WATRES.2022.118860

Wu, S., Tetzlaff, D., Goldhammer, T., & Soulsby, C. (2021). Hydroclimatic variability and riparian wetland restoration control the hydrology and nutrient fluxes in a lowland agricultural catchment. *Journal of Hydrology*, *603*, 126904. https://doi.org/10.1016/J.JHYDROL.2021.126904

Wu, S., Tetzlaff, D., Yang, X., & Soulsby, C. (2022). Identifying dominant processes in time and space: Time-varying spatial sensitivity analysis for a grid-based nitrate model. *Water Resources Research*, *58*, e2021WR031149. https://doi.org/10.1029/2021WR031149

Xie, Y., Sha, Z., & Yu, M. (2008). Remote sensing imagery in vegetation mapping: A review. *Journal of Plant Ecology*, *1*, 9–23. https://doi.org/10.1093/JPE/RTM005

Yan, Y., Deng, H., Liu, Y., & Zhu, L. (2019). Application of UAV-based multi-angle hyperspectral remote sensing in fine vegetation classification. *Remote Sensing*, *11*, 2753. https://doi.org/10.3390/rs11232753

Yeom, J., Jung, J., Chang, A., Ashapure, A., Maeda, M., Maeda, A., & Landivar, J. (2019). Comparison of vegetation indices derived from UAV data for differentiation of tillage effects in agriculture. *Remote Sensing*, *11*, 1548. https://doi.org/10.3390/RS11131548

Yu, F., Price, K. P., Ellis, J., & Shi, P. (2003). Response of seasonal vegetation development to climatic variations in eastern Central Asia. *Remote Sensing of Environment*, *87*, 42–54. https://doi.org/10.1016/S0034-4257(03)00144-5

Zaman, B., McKee, M., & Neale, C. M. U. (2012). Fusion of remotely sensed data for soil moisture estimation using relevance vector and support vector machines. *International Journal of Remote Sensing*, *33*, 6516–6552. https://doi.org/10.1080/01431161.2012.690540

Zhang, X., Zhang, F., Qi, Y., Deng, L., Wang, X., & Yang, S. (2019). New research methods for vegetation information extraction based on visible light remote sensing images from an unmanned aerial vehicle (UAV). *International Journal of Applied Earth Observation and Geoinformation*, *78*, 215–226. https://doi.org/10.1016/j.jag.2019.01.001

Zweig, C., Percival, H., Burgess, M., & Kitchens, W. (2015). Use of unmanned aircraft systems to delineate fine-scale wetland vegetation communities. *Wetlands*, *35*, 303–309. https://doi.org/10.1007/s13157-014-0612-4

SUPPORTING INFORMATION

Additional supporting information can be found online in the Supporting Information section at the end of this article.

How to cite this article: Wu, S., Tetzlaff, D., Daempfling, H., & Soulsby, C. (2023). Improved understanding of vegetation dynamics and wetland ecohydrology via monthly UAV-based classification. *Hydrological Processes*, *37*(9), e14988. https://doi.org/10.1002/hyp.14988